Published in Chemical Physics Letters 397(4-6): 441-446, 2004

Application of the density functional theory derived orbital-free embedding potential to calculate the splitting energies of lanthanide cations in chloroelpasolite crystals

Mohamed Zbiri [a], Mihail Atanasov [a,b], Claude Daul [a], Juan Maria Garcia-Lastra [c], Tomasz A. Wesolowski [d,*]

[a] *Département de Chimie, Université de Fribourg – Ch. du Musée, CH-1700 Fribourg, Switzerland*
[b] *Institute of General and Inorganic Chemistry, Bulgarian Academy of Sciences, Acad. G. Bontchev Str.Bl.11, 1113 Sofia, Bulgaria*
[c] *Departamento de Física Moderna, Universidad de Cantabria – Facultad de Ciencias, Avda de los Castros, Santander C.P. 39005, Spain*
[d] *Département de Chimie, Université de Genève - 30, quai Ernest-Ansermet, CH-1211 Genève. 4, Switzerland*

Received 5 August 2004; in final form 3 September 2004

Abstract

Ligand field splitting energies of lanthanides Ln^{3+} (Ln = from Ce to Yb) in octahedral environment are calculated using the Hohenberg–Kohn theorems based orbital-free embedding formalism. The lanthanide cation is described at orbital level whereas its environment is represented by means of an additional term in the Kohn–Sham-like one-electron equations expressed as an explicit functional of two electron densities: that of the cation and that of the ligands. The calculated splitting energies, which are in good agreement with the ones derived from experiment, are attributed to two main factors: (i) polarization of the electron density of the ligands, and; (ii) ion–ligand Pauli repulsion.

1. Introduction

Theoretical modelling of confined systems such as an atom, an ion, or a molecule in condensed phase, presents usually a challenging task. The object of primary interest interacts with its microscopic environment which comprises usually a large number of atoms. Describing the whole such system at a high-end quantum mechanical level is usually not practical. In the early days of quantum mechanics, Sommerfeld and Welker [1] put forward the idea of *confining potential* (or *embedding potential*) to be added to the Hamiltonian of the isolated subsystem of interest in order to represent its interactions with the environment. The idea of the embedding potential found a large number of practical implementations varying in degree of their range of applicability and the extend of the use of empirical parameters [2–5]. Crystal field theory can be seen as a particular version of the embedding strategy in which the environment of an ion in the crystal lattice is represented only by its electrostatic field. This simple model proved to be not sufficiently accurate which resulted in the development of the ligand-field theory in which non-electrostatic effects are taken into account. Such effects are represented using orbital-level representation of the environment of the ion [6]. The non-electrostatic contributions to the embedding potential for an ion in the crystal lattice are significant but can be approximated by a simple empirical overlap dependent term [7] or more sophisticated empirical ligand pseudopotentials such as the ones used recently in studies of ligand-field splitting in lanthanides [8].

* Corresponding author.
E-mail address: Tomasz.Wesolowski@chiphy.unige.ch (T.A. Wesolowski).

0009-2614
doi:10.1016/j.cplett.2004.09.010

Hohenberg–Kohn theorems [9] provide a general theoretical framework to construct the first-principles based embedding potential [10]. The electron density of a subsystem (ρ_I) embedded in a given microscopic environment (ρ_{II}) can be derived form a constrained minimization of the total energy bi-functional $E[\rho_I, \rho_{II}]$ keeping ρ_{II} frozen. In this work, a new type of application of this formalism is reported-the studies of the electronic structure of embedded lanthanide ions. It is its first application to f-elements. Lanthanide chloroelpasolites, $Cs_2NaLnCl_6$ (Ln = lanthanide) are very suitable objects for the study of the applicability of the orbital-free embedding formalism to f-elements owing to the rich collection of data concerning their properties [11–13].

The principal objective of this work is the exploration of a new area of applicability (f-elements) of the developed approximations to the orbital-free embedding potential. The second objective of this work is the assessment of relative importance of various contributions to the splitting energy, such as electrostatic interactions with not-polarized ligands, electric polarization of the ligands, and the non-electrostatic overlap-dependent effects, and orbital interactions.

2. Computational details

The minimization of the total-energy bi-functional $E[\rho_I, \rho_{II}]$, where ρ_I and ρ_{II} correspond to the electron density of the cation and the ligands, respectively, is performed by means of the Kohn–Sham-like equations [10]

$$\left[-\frac{1}{2}\nabla^2 + V_{\text{eff}}^{\text{KSCED}}[\vec{r}, \rho_I, \rho_{II}]\right]\phi_{(I)i} = \epsilon_{(I)i}\phi_{(I)i}, \tag{1}$$

where $\rho_I = \sum_i |\phi_{(I)i}|^2$, and $V_{\text{eff}}^{\text{KSCED}}[\vec{r}, \rho_I, \rho_{II}]$ is the sum of the Kohn–Sham effective potential for the isolated subsystem [14] ($V^{\text{KS}}[\vec{r}, \rho_I]$) and the orbital-free embedding effective potential given by

$$\begin{aligned} V_{\text{emb}}^{\text{eff}}[\vec{r}, \rho_I, \rho_{II}] = \sum_{A_{II}} -\frac{Z_{A_{II}}}{|\vec{r} - \vec{R}_{A_{II}}|} + \int \frac{\rho_{II}(\vec{r}')}{|\vec{r}' - \vec{r}|}\,\mathrm{d}\vec{r}' \\ + \frac{\delta E_{xc}[\rho_I + \rho_{II}]}{\delta\rho_I} - \frac{\delta E_{xc}[\rho_I]}{\delta\rho_I} \\ + \frac{\delta T_s^{\text{nad}}[\rho_I, \rho_{II}]}{\delta\rho_I}, \end{aligned} \tag{2}$$

where $T_s^{\text{nad}}[\rho_I, \rho_{II}] = T_s[\rho_I + \rho_{II}] - T_s[\rho_I] - T_s[\rho_{II}]$, the functionals $E_{xc}[\rho]$, and $T_s[\rho]$ are defined in the Kohn–Sham formalism [14].

Both $V^{\text{KS}}[\vec{r}, \rho_I]$ and $V_{\text{emb}}^{\text{eff}}[\vec{r}, \rho_I, \rho_{II}]$ do not depend on the orbitals but only on the electron densities of the two subsystems. They are, therefore, *orbital-free*. It is worthwhile to notice that the orbital-free embedding formalism can be seen as a particular application of the subsystem-based formulation of density functional theory [15] for two subsystems which might be described using different levels of approximation. Applying the orbital-free embedding formalism to derive f-level splitting energies can be also seen as a non-empirical realization of the original ideas of Schäffer and Jørgensen [17] developed further by Urland [18].

Gradient-dependent functionals approximating $T_s^{\text{nad}}[\rho_I, \rho_{II}]$ and $E_{xc}[\rho]$ make it possible to study only such systems for which the overlap between ρ_I and ρ_{II} is small [19]. See [16] for review of recent applications. In this work, we use the approximate functionals which were chosen based on dedicated studies concerning $T_s^{\text{nad}}[\rho_I, \rho_{II}]$ [19] and the whole bi-functional $E[\rho_I, \rho_{II}]$ [20].

Fig. 1 represents the investigated system comprising an octahedral arrangement of the lanthanide cation and its ligands (O_h symmetry). The lanthanide–ligand distances derived from ab initio (CASSCF or CASPT2) cluster calculations [21] were used.

The principal results were obtained using ρ_{II} minimizing the total-energy bi-functional $E[\rho_I, \rho_{II}]$ in Eq. (2) in the 'freeze-and-thaw' cycle of iterations [22]. This density is labeled as *relaxed* ρ_{II} throughout this work. Relativistic scalar ZORA [23], all electron calculations were performed using the ZORA triple-ζ STO set plus one polarization function [24]. The van Leeuwen–Baerends (LB94) exchange-correlation potential [25] was used to

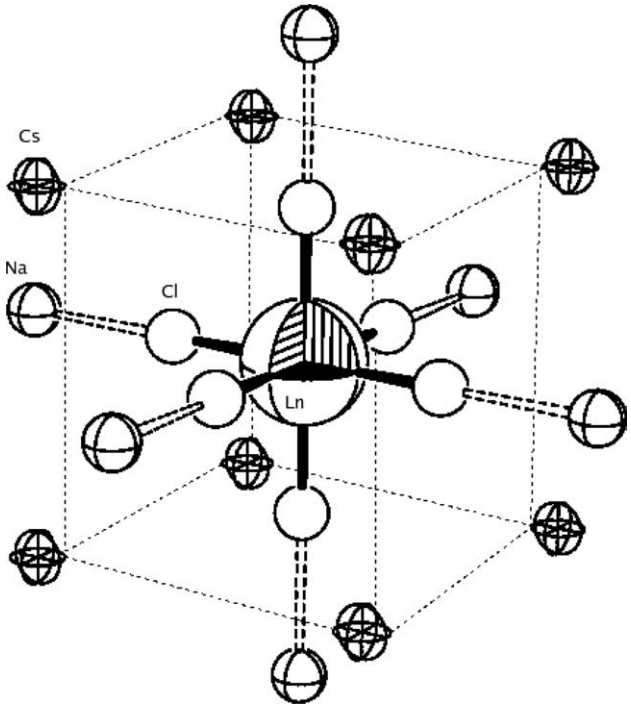

Fig. 1. Schematic view on the environment of studied lanthanide cations. Each Ln^{3+} is hexacoordinated to six Cl^- ions. The second coordinations sphere comprises eight Cs^+ ions at the corners of the cube. The third coordination sphere comprises six Na^+ ions occupying the vertices of the octahedron.

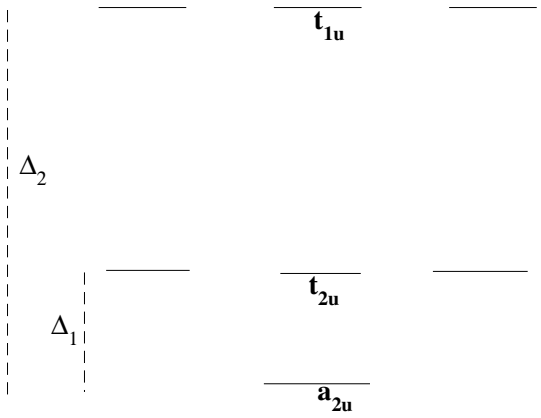

Fig. 2. The f-orbital levels of Ln^{3+} in the octahedral environment.

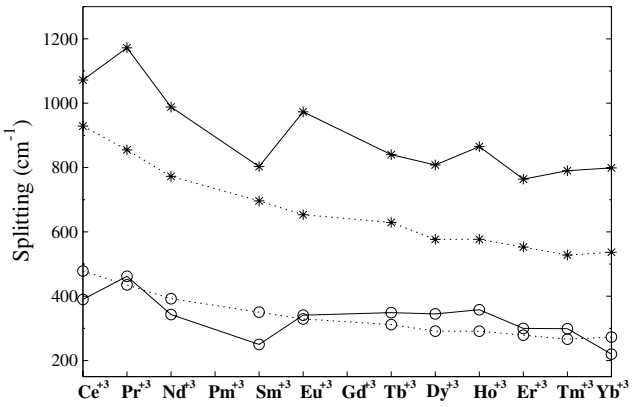

Fig. 3. Ligand field splitting parameters (Δ_1 and Δ_2) in the octahedrally coordinated lanthanide ions: the splitting energies calculated using effective embedding potential of Eq. (2) and *relaxed* ρ_{II} and the observed splitting energies. Calculations were made at the ab initio optimized ion–ligand distances taken from the literature. Solid and dotted lines are used to guide the eye for experimental [11] and calculated results,respectively. Circles and stars indicate Δ_1 and Δ_2, respectively.The estimated error bars of experimental parameters are not shown because they are of the size of the applied symbols.

approximate the exchange-correlation component of $V^{KS}[\vec{r}, \rho_I]$ in Eq. (1). This choice was motivated by the fact that the ligands are negatively charged and such systems are not well described by means of Kohn–Sham equations applying local and semi-local functionals. The computer code performing orbital-free embedding calculations (Eqs. (1) and (2)) based on the ADF package (version 2003.01) was used [26].

The ligand field splitting parameters Δ_1 and Δ_2 analyzed throughout this work are also defined in Fig. 2. They were calculated for average-of-configuration (AOC) in which each f-orbital was partially occupied (occupation number $n/7$ for a given f^n configuration). Table 1 collects data concerning the geometry and the electronic configuration for each lanthanide cation. The experimental ligand field parameters Δ_1 and Δ_1 were taken from [11].

3. Results and discussion

Fig. 3 shows our principal results obtained using *relaxed* ρ_{II} in Eq. (2). In the whole series, the calculated values of the parameter Δ_1 are in a very good agreement with experiment. The experimental values decrease almost mono-tonically in the whole series from 380 cm^{-1} (Ce) to 220 cm^{-1} (Yb). The dependence of calculated Δ_1 on the number of f-electrons is, however, smoother than that deduced from experimental data. The average and the maximal deviation from experimental data amount to 30 and 100 cm^{-1} (Sm), respectively. These rather small discrepancies between these two sets of parameters can be attributed to various factors (see the discussion later). Fig. 3 shows that the calculated and experimental values of Δ_2 are also in a rather good agreement.The average and the maximal deviation from experimental data amount to 185 and 320 cm^{-1} (Sm), respectively. As in the case of Δ_1 the dependence of calculated values of Δ_2 on the number of f-electrons is smoother than that deduced from experimental data. For Δ_2, however, the calculated values underestimate the experimental results by about 200 cm^{-1}. In the following section, the factors which might contribute to the discrepancies between the ligand-field parameters deduced from experimental data and that calculated in this work are discussed.

The discrepancy between the experimental and calculated data might originate either from: (a) the intrinsic error of the applied exchange-correlation functional which could lead to different errors of the orbital-energies of different symmetry (see the detailed analysis of this issue in [28]); (b) the errors in the applied approximate embedding effective potential leading to a not adequate description of the cation–ligand Pauli repul-

Table 1
Electronic configuration of the lanthanide ions and the Ln–Cl bond lengths used in the calculations: [a]the sum of the ionic radii and [b]the ab initio optimized bond length

	Ce^{3+}	Pr^{3+}	Nd^{3+}	Pm^{3+}	Sm^{3+}	Eu^{3+}	Gd^{3+}	Tb^{3+}	Dy^{3+}	Ho^{3+}	Er^{3+}	Tm^{3+}	Yb^{3+}
f-Shell occupation	f^1	f^2	f^3	f^4	f^5	f^6	f^7	f^8	f^9	f^{10}	f^{11}	f^{12}	f^{13}
Ionic radii[a]	2.82	2.8	2.793	2.78	2.768	2.757	2.748	2.733	2.722	2.711	2.7	2.69	2. 678
CASPT2/AIMP[b]	2.682	2.666	2.656	2.642	2.631	2.630	2.609	2.595	2.584	2.571	2.567	2. 556	2.544

[a] Sum of ionic radii [$r(Ln^{3+}) + r(Cl^-)$] from [27].
[b] CASPT2 values of $d(Ln^{3+}–Cl^-)$ from [21].

sion; (c) the use of AOC to derive the orbital energies; (d) inadequacies of our model (its size and geometry). The most striking feature is a rather uniform underestimation of Δ_2 suggesting a common origin. We attribute this underestimation to the redistribution of the electron density ρ_{II} corresponding to some ligand-to-cation charge transfer. Such an effect was neglected in our calculations in which ρ_{II} was localized on the ligands. The transfer of charge density would increase the levels of the orbitals because it would cause the increase of the repulsive non-additive kinetic energy component of the effective embedding potential. The remaining discrepancies (the lack of peaks in the theoretical curves) could be attributed also to the other factors. In particular, using AOC might lead to two types of errors. One related to orbital relaxation and another to the different errors in the energies of t_{1u}, t_{2u} and a_{2u} orbitals derived from calculations using approximate exchange-correlation potential. As far as the orbital relaxation is concerned, they were estimated previously and amount to only 1–2% of the excitation energy [29]. The model-related factors, such as the assumed geometry of the investigated systems and the long-range effects (the contributions due to atoms beyond the second coordination shell) might also contribute to the apparent discrepancy. The geometry of the lanthanide centers in chloroelpasolite crystals, $Cs_2NaLnCl_6$, cannot be obtained in direct measurements. Unfortunately, even a small change in the lanthanide–ligand bond length results in a large change in the optical parameters of the embedded cation (dependence as $1/d^n_{Ln-Cl}$ with $n = 5$–6). To estimate the magnitude of the possible effect of the geometry, the ligand-field parameters were recalculated using the sum-of-ionic-radii geometries instead of ab initio optimized geometries [21]. The change of the geometry does not affect significantly our results. The maximal effect occurs for Ce, where Δ_1 changes from 478 to 391 cm^{-1} and for Nd, where Δ_2 changes from 763 to 626 cm^{-1}. The effect of beyond-the-second-coordination-shell atoms can be determined in a straightforward manner. The electrostatic potential generated by 142 point charges was added to the external potential in Eq. (2). The charges were chosen to reproduce the electric field corresponding to the infinite system (Madelung potential). Adding this field, however, did not result in any noticeable effect on the calculated parameters.

Five simplified methods to describe the environment, which can be seen as approximations to the full orbital-free embedding potential discussed so far, are analyzed below:

(A) *Point charge embedding*. The environment of the ion comprising a set of point charges representing the nearest neighbors of the lanthanide cation in the crystal: six negative charges ($q_{Cl} = -1e$), eight positive charges ($q_{Cs} = +1e$), and six positive charges ($q_{Na} = +1e$). This model can be seen as a simplification of Eq. (2) in which all non-electrostatic terms are neglected and the terms representing Coulomb interactions are approximated by a truncated multicenter multipole expansion.

(B) *Electrostatics-only embedding with not-polarized* ρ_{II}. (i.e. calculated by means of Kohn-Sham equations for the isolated ligands.) In this model, the Coulomb interactions are calculated exactly for a given ρ_{II} but all non-electrostatic terms in Eq. (2) are neglected.

(C) *Electrostatics-only embedding with pre-polarized* ρ_{II}. (i.e. calculated by means of Kohn-Sham equations for the ligands in the presence of a +3a point charge mimicking the cation.) In this model, the Coulomb interactions are calculated exactly for a given ρ_{II} but all non-electrostatic terms Eq. (2) are neglected.

(D) *Eq. (2) embedding with not-polarized* ρ_{II}.

(E) *Eq. (2) embedding with pre-polarized* ρ_{II}.

Table 2 collects all the results obtained using the simplified models (A–E). The results shown in Fig. 3 are also given for comparison. For simplified embedding potentials A and D, the splitting energies are almost the same. The calculated splitting energies, underestimate significantly (by the factor of 2–3) the experimental ones. It indicates, that other factors must be taken into account. Comparison between the results obtained using the embedding potential of Eq. (2) with two different ρ_{II}, either *relaxed* or *not-polarized* (effective potential D), shows that the polarization of the environment (ligands) plays a key role in determining the magnitude of the splitting energies. Allowing the ligands to become polarized by the cation results in a significant increase of the magnitude of the splitting energies and brings them close to experimental values. The results collected in Table 2 show clearly that the overlap-dependent terms are indispensable in the embedding potential. Without them the environment induced shifts of f-levels are quantitatively (models A, D) and qualitatively (reverse ordering of levels, models C, B) wrong. The results derived using *relaxed* ρ_{II} and *pre-polarized* ρ_{II} in Eq. (2) are very similar. They differ by less than 30 cm^{-1}. This indicates a possible additional saving in the overall time of computations because the 'freeze-and-thaw' cycle can be avoided.

For the systems considered in this work (lanthanide cation and its ligands), the conventional supermolecule Kohn–Sham calculations are possible. Unfortunately, the splitting energies derived from such calculations are not satisfactory [30]. The numerical results derived from embedding calculations are clearly superior to that derived from supermolecular Kohn–Sham results for the whole system. We attribute the superiority of the embedding results to the fact that the Kohn–Sham orbitals

Table 2
The values of the Δ_1 and Δ_2 parameters in (cm^{-1}) from experiment, derived from 'freeze-and-thaw' orbital-free embedding calculations (Eq. (2) with *relaxed* ρ_{II}), and derived from calculations using simplified embedding schemes

		Ce	Pr	Nd	Pm	Sm	Eu	Gd	Tb	Dy	Ho	Er	Tm	Yb
Experiment	Δ_1	390	462	343	–	250	341	–	349	345	358	300	299	220
	Δ_2	1072	1172	988	–	803	973	–	840	808	865	764	790	799
Eq. (2) *Relaxed* ρ_{II}	Δ_1	478	435	392	365	350	329	312	312	291	291	279	266	273
	Δ_2	929	855	773	725	696	653	620	629	576	577	553	528	537
Eq. (2) *Pre-polarized* ρ_{II}	Δ_1	487	441	396	368	351	329	311	309	287	286	273	260	264
	Δ_2	926	848	763	714	682	638	602	609	555	552	528	503	507
Eq. (2) *not-polarized* ρ_{II}	Δ_1	210	188	166	153	146	137	126	127	115	116	110	104	108
	Δ_2	391	359	318	297	285	267	248	261	227	229	219	207	211
Point charge embedding	Δ_1	189	171	154	141	135	128	118	119	108	106	102	96	100
	Δ_2	404	362	323	292	280	263	241	252	217	214	204	191	197
Electrostatic-only embedding	Δ_1	25	7	−4	−9	−18	−20	−25	−30	−33	−37	−34	−33	−40
pre-polarized ρ_{II}	Δ_2	−1066	−672	−515	−382	−347	−297	−265	−244	−228	−224	−193	−172	−191
Electrostatic-only embedding	Δ_1	−77	−87	−91	−92	−98	−97	−99	−102	−101	−105	−100	−97	−103
not-polarized ρ_{II}	Δ_2	−945	−711	−596	−492	−463	−417	−385	−364	−347	−342	−310	−287	−303

derived using local or semi-local approximations to the exchange-correlation potential mix too strongly the f-orbitals of lanthanides with the orbitals of the ligands [31]. Opposite to the supermolecule Kohn–Sham calculations, the orbital-level description is restricted to a selected subsystem in the orbital-free embedding calculations. The artificial over-estimation of covalency in Kohn–Sham calculations using current exchange-correlation functionals is, therefore, less pronounced in the subsystem-based calculations.

4. Conclusions

The numerical values of the splitting energies derived from the orbital-free effective embedding potential of Eq. (2) and approximated using the relevant gradient-dependent density functional [20] describes rather accurately (with the relative error of less than 20%) the effect of the ligand on the f-orbital levels. The reported study is the first one in which the approximations to the overlap-dependent terms in the orbital-free embedding effective potential used so far only for s-, p- and d- elements is applied to f-elements.

Despite the well known fact that lanthanide–ligand bonds have ionic character in such systems, the detailed analysis shows that a quantitative description of the f-level splitting energy results not from simple electrostatic interactions between the ion and the not-polarized ligands but from two dominant effects:one associated with the strong polarization of the ligands by the cation and the other originating from the repulsive interactions between overlapping electron densities of the cation and its ligands. Neglecting either of these effects worsens qualitatively the accuracy of the calculated ligand-field splitting parameters. In particular, the electrostatic interactions between the lanthanide cation and the not-polarized ligands lead to splitting energies which are 2–3 times too small.

Acknowledgement

This work is supported by the Swiss National Science Foundation (Projects 21-63645.00 and 200020-100411/1). It is also part of the COST D26 Action.

References

[1] A. Sommerfeld, H. Welker, Ann. Phys. 32 (1938) 56.
[2] J. Åqvist, A. Warshel, Chem. Rev. 93 (1993) 2523.
[3] J. Gao, in: K.B. Lipkowitz, D.B. Boyd (Eds.), Reviews in Computational Chemistry, vol. 7, VCH Publishers, New York, 1996, p. 119.
[4] J. Sauer, P. Ugliengo, E. Garrone, V.R. Sounders, Chem. Rev. 94 (1994) 2095.
[5] W. Jaskólski, Phys. Rep. 271 (1996) 1.
[6] C.J. Ballhausen, J.P. Dahl, Theor. Chim. Acta 34 (1974) 169.
[7] C. Domene, P.W. Fowler, P.A. Madden, M. Wilson, R.J. Wheatley, Chem. Phys. Lett. 314 (1999) 158.
[8] J. Ren, M.-H. Whangbo, D. Dai, L. Li, J. Chem. Phys. 108 (1998) 8479.
[9] P. Hohenberg, W. Kohn, Phys. Rev. 136 (1964) B864.
[10] T.A. Wesolowski, A. Warshel, J. Phys. Chem. 97 (1993) 8050.
[11] F.S. Richardson, M.F. Reid, J.J. Dallara, R.D. Smith, J. Chem. Phys. 83 (1985) 3813.
[12] M. Bettinelli, R. Moncorge, J. Lumin. 92 (2001) 287.
[13] P. Dorenbos, J. Lumin. 91 (2000) 155.
[14] W. Kohn, L.J. Sham, Phys. Rev. 140 (1965) A1133.
[15] P. Cortona, Phys. Rev. B 44 (1991) 8454.

[16] T.A. Wesolowski, CHIMIA 56 (2003) 707.
[17] C.E. Schäffer, C.K. Jørgensen, Mol. Phys. 9 (1965) 401.
[18] W. Urland, Chem. Phys. 14 (1976) 393.
[19] T.A. Wesolowski, J. Chem. Phys. 106 (1997) 8516.
[20] T.A. Wesolowski, F. Tran, J. Chem. Phys. 118 (2003) 2072.
[21] B. Ordejón, L. Seijo, Z. Barandiarán, J. Chem. Phys. 119 (2003) 6143.
[22] T.A. Wesolowski, J. Weber, Chem. Phys. Lett. 248 (1996) 71.
[23] E. van Lenthe, R. van Leeuwen, E.J. Baerends, J.G. Snijders, Int. J. Quantum Chem. 57 (1996) 281.
[24] E. van Lenthe, E.J. Baerends, J. Comput. Chem. 24 (2003) 1142.
[25] R. van Leeuwen, E.J. Baerends, Phys. Rev. A 49 (1994) 2421.
[26] ADF 2003.01, SCM, Theoretical Chemistry, Vrije Universiteit, Amsterdam, The Netherlands. Available from <http://www.scm.com> (modified to perform orbital-free embedding calculations).
[27] R.D. Shanon, Acta Crystallogr., Sec. A: Cryst. Phys., Diff. Theor., Gen. Crystallogr. 32 (1976) 751.
[28] E.J. Baerends, V. Branchadell, M. Sodupe, Chem. Phys. Lett. 265 (1997) 481.
[29] M. Atanasov, C. Daul, C. Rauzy, Struct. Bond. 106 (2004) 97.
[30] M. Atanasov, C. Daul, H.U. Güdel, T.A. Wesolowski, M. Zbiri, to be published.
[31] M. Atanasov, C.A. Daul, H.U. Güdel, in: J. Leszczynski (Ed.), Computational Chemistry: Reviews of Current Trends, vol. 9, World Scientific Publishing Company, Singapore, 2004.